

---

# Scaling up the Automatic Statistician: Scalable Structure Discovery using Gaussian Processes

---

**Hyunjik Kim**

Department of Statistics  
University of Oxford  
hkim@stats.ox.ac.uk

**Yee Whye Teh**

Department of Statistics  
University of Oxford  
y.w.teh@stats.ox.ac.uk

## Abstract

Automating statistical modelling is a challenging problem that has far-reaching implications for artificial intelligence. The Automatic Statistician employs a kernel search algorithm to provide a first step in this direction for regression problems. However this does not scale due to its  $O(N^3)$  running time for the model selection. This is undesirable not only because the average size of data sets is growing fast, but also because there is potentially more information in bigger data, implying a greater need for more expressive models that can discover finer structure. We propose Scalable Kernel Composition (SKC), a scalable kernel search algorithm, to encompass big data within the boundaries of automated statistical modelling.

## 1 Introduction

Automated statistical modelling is an area of research in its early stages, yet it is becoming an increasingly important problem. As a growing number of disciplines use statistical analyses and models to help achieve their goals, the demand for statisticians, machine learning researchers and data scientists is at an all time high. Automated systems for statistical modelling aim to serve as an assistant to help increase the efficiency of these human resources, if not as a best alternative where there is a shortage.

Duvenaud et al [9] take the first step of tackling the problem of structure discovery in nonparametric regression by fitting a Gaussian Process (GP) to the data, with an algorithm for automatically choosing a suitable parametric form of the kernel. This leads to high predictive performance that matches those with kernels hand-selected by GP experts [25]. There also exist other approaches that tackle this model selection problem by using a more flexible kernel [1, 22, 28, 37, 38]. However the distinctive feature of [9] is that the resulting models are interpretable; the kernels are constructed in such a way that we can use them to describe patterns in the data, and thus can be used for automated exploratory data analysis. [17] exploit this to generate natural language analyses from these kernels, a procedure which they name Automatic Bayesian Covariance Discovery (ABCD). The Automatic Statistician<sup>1</sup> implements this to output a 10-15 page report when given data input.

However, a limitation of ABCD is that it does not scale; due to the  $O(N^3)$  time for inference in GPs, the analysis is constrained to small data sets, specialising in one dimensional time series data. This is a grave drawback in this era when data is getting bigger and more high dimensional. Moreover it is clear that the importance of model selection increases with the size of the data set; we would like to select a more expressive model that adequately captures the information in the bigger data. This paper proposes SKC, a scalable extension to the Compositional Kernel Search (CKS) algorithm of ABCD, to push the boundaries of automated statistical modelling to bigger data. In summary, our work makes the following contributions:

---

<sup>1</sup>See <http://www.automaticstatistician.com/index/> for example analyses

- We propose the first scalable and highly parallelisable version of the Automatic Statistician.
- We derive a novel cheap upper bound to the GP marginal likelihood, which is in particular tighter than the lower bound in [34], considered state of the art for scalable GP marginal likelihood approximation.
- We give extensive experimental results that give insight into the behaviour of our upper bound and the lower bound.

## 2 Automatic Bayesian Covariance Discovery (ABCD) and Compositional Kernel Search (CKS)

The Compositional Kernel Search (CKS) algorithm in [9] builds on the idea that the sum and product of two positive definite kernels are also positive definite. Starting off with a set  $\mathcal{B}$  of base kernels defined on  $\mathbb{R} \times \mathbb{R}$ , the algorithm searches through the space of zero-mean GPs with kernels that can be expressed in terms of sums and products of these base kernels. The base set  $\mathcal{B} = \{\text{SE}, \text{LIN}, \text{PER}\}$  is used, which correspond to the squared exponential, linear and periodic kernel respectively (the exact form of these base kernels are given in Appendix C). Thus candidate kernels form an open-ended space of GP models, allowing for an expressive model. Such approaches for structure discovery have also appeared in [11, 12]. A greedy search is employed to explore this space, with each kernel scored by the Bayesian Information Criterion (BIC) [29]<sup>2</sup> after optimising the kernel hyperparameters by type II maximum likelihood (ML-II). See Appendix B for the algorithm in detail.

The resulting kernel can be simplified to be expressed as a sum of products of base kernels, which has the remarkable benefit of interpretation. In particular, note  $f_1 \sim GP(0, k_1), f_2 \sim GP(0, k_2) \Rightarrow f_1 + f_2 \sim GP(0, k_1 + k_2)$  for independent  $f_1$  and  $f_2$ . So a GP whose kernel is a sum of products of kernels can be interpreted as sums of GPs each with structure given by the product of kernels. Now each base kernel in a product modifies the model in a consistent way. For example, multiplication by SE converts global structure into local structure since  $\text{SE}(x, x')$  decreases exponentially with  $|x - x'|$ , and multiplication by PER is equivalent to multiplication of the modeled function by a periodic function (see [17] for detailed interpretations for different base kernels). [17] use this observation for ABCD, giving a natural language description of the resulting function modeled by the composite kernel. In summary ABCD consists of two algorithms: the compositional kernel search CKS, and the natural language translation of the kernel into a piece of exploratory data analysis.

## 3 Scaling up ABCD

ABCD provides a framework for a natural extension to big data settings, in that we only need to be able to scale up CKS, then the natural language description of models can be directly applied. The difficulty of this extension of CKS to big data settings lies in the  $O(N^3)$  time for evaluation of the GP marginal likelihood and its gradients with respect to the kernel hyperparameters. A naïve approach is to subsample the data to reduce  $N$ , but then we may fail to capture global structure such as periodicities with long periods or omit a set of points displaying a certain local structure. Alternatively it is tempting to use either an approximate marginal likelihood or the exact marginal likelihood of an approximate model as a proxy for the exact likelihood [23, 30, 32, 34]. However such scalable GP methods are limited in interpretability as they often behave very differently to the full GP, lacking guarantees for the chosen kernel to faithfully reflect the actual structure in the data. In other words, the real challenge is to scale up the GP while preserving interpretability. Our approach is as follows: we provide a cheap lower and upper bound to sandwich the exact marginal likelihood, and we use this interval for model selection. To do so we give a brief overview of the relevant work on low rank kernel approximations used for scaling up GPs, and we later outline how they can be applied to obtain cheap lower and upper bounds.

### 3.1 Nyström Methods and Sparse Gaussian Processes

The Nyström Method [8, 36] selects a set of  $m$  inducing points in the input space  $\mathbb{R}^D$  that attempt to explain all the covariance in the Gram matrix of the kernel; the kernel is evaluated for each pair of

<sup>2</sup>BIC = log marginal likelihood with a model complexity penalty. We use a formulation where higher BIC means better model fit. See Appendix A

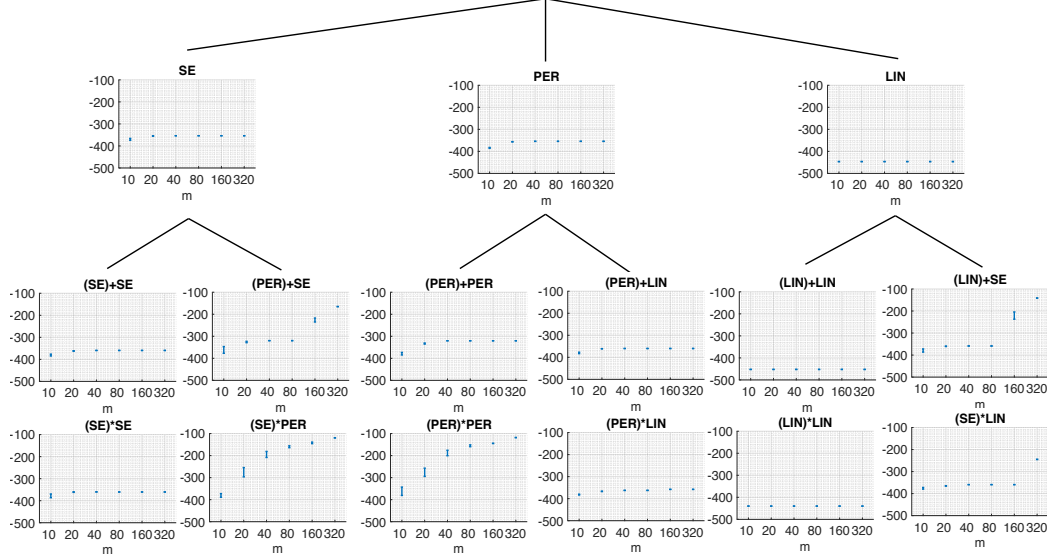


Figure 1: Kernel search tree for SKC on solar data up to depth 2. We show the upper and lower bounds for different numbers of inducing points  $m$ .

inducing points and also between the inducing points and the data, giving matrices  $K_{mm}, K_{mn} = K_{nm}^\top$ . This is used to create the Nyström approximation  $\hat{K} = K_{nm}(K_{mm})^\dagger K_{mn}$  of  $K$ , where  $\dagger$  is the pseudo-inverse. Applying Cholesky decomposition to  $K_{mm}$ , we see that the approximation admits the low-rank form  $\Phi^\top \Phi$  and so allows efficient computation of determinants and inverses in  $O(m^2N)$  time (see Appendix D). We later use the Nyström approximation to give an upper bound on the exact marginal likelihood.

The Nyström approximation arises naturally in the sparse GP literature, where certain distributions are approximated by simpler ones involving  $\mathbf{f}_m$ , the GP evaluated at the  $m$  inducing points: the DTC approximation [30] defines a model that gives the marginal likelihood  $q(\mathbf{y}) = \mathcal{N}(\mathbf{y}|0, \hat{K} + \sigma^2 I)$  ( $\mathbf{y}$  is the vector of observations), whereas the FIC approximation [32] gives  $q(\mathbf{y}) = \mathcal{N}(\mathbf{y}|0, \hat{K} + \text{diag}(K - \hat{K}) + \sigma^2 I)$ , correcting the Nyström approximation along the diagonals. [23] further improves this by introducing the PIC approximation, where the Nyström approximation is corrected on block diagonals with blocks typically of size  $m \times m$ . Note that the approximation is no longer low rank for FIC and PIC, but matrix inversion can still be computed in  $O(mN^2)$  time by Woodbury’s Lemma (see Appendix D).

The variational inducing points method (VAR) introduced by [34] is rather different to DTC/FIC/PIC in that it gives the following variational lower bound on the exact log marginal likelihood:

$$\log[\mathcal{N}(\mathbf{y}|0, \hat{K} + \sigma^2 I)] - \frac{1}{2\sigma^2} \text{Tr}(K - \hat{K}) \quad (1)$$

This lower bound is optimised with respect to the inducing points and the kernel hyperparameters, which is shown in [34] to successfully yield tight lower bounds in  $O(Nm^2)$  time for reasonable values of  $m$ . Another useful property of VAR is that the lower bound can only increase as the set of inducing points grows [19, 34]. [3] also point out that VAR always improves with extra computation, and that it successfully recovers the true posterior GP in most cases, contrary to other sparse GP methods. Hence this is what we use in the scalable structure discovery to obtain a lower bound on the marginal likelihood and optimise the hyperparameters. We use 10 random initialisations of hyperparameters and choose the one with highest lower bound after optimisation. Also note that contrary to DTC/FIC/PIC, (1) cannot be seen as the log marginal likelihood with a plug-in estimate for the Gram matrix.

### 3.2 A Cheap and Tight Upper Bound on the Marginal Likelihood

Fixing the hyperparameters to be those tuned by VAR, we seek a cheap upper bound to the exact marginal likelihood. Upper bounds and lower bounds are qualitatively different, and in general it

is more difficult to obtain an upper bound than a lower bound for the following reason: first note that the marginal likelihood is the integral of the likelihood with respect to the prior density of parameters. Hence to obtain a lower bound it suffices to exhibit regions in the parameter space giving high likelihood. On the other hand, to obtain an upper bound one must demonstrate the absence or lack of likelihood mass outside a certain region, an arguably more difficult task. There has been some work on the subject [4, 15], but to the best of our knowledge there has not been any work on cheap upper bounds to the marginal likelihood in large  $N$  settings. So finding an upper bound from the perspective of the marginal likelihood can be difficult. Instead, we exploit the fact that the GP marginal likelihood has an analytic form, and treat it as a function of  $K$ .

The GP log marginal likelihood is composed of two terms and a constant:

$$\log p(y) = \log[\mathcal{N}(y|0, K + \sigma^2 I)] = -\frac{1}{2} \log \det(K + \sigma^2 I) - \frac{1}{2} y^\top (K + \sigma^2 I)^{-1} y - \frac{N}{2} \log(2\pi) \quad (2)$$

We give separate upper bounds on the negative log determinant (NLD) term and the negative inner product (NIP) term. For NLD, [2] prove that

$$-\frac{1}{2} \log \det(K + \sigma^2 I) \leq -\frac{1}{2} \log \det(\hat{K} + \sigma^2 I) \quad (3)$$

a consequence of  $K - \hat{K}$  being positive semi-definite. Hence the Nyström approximation plugged into the NLD term serves as an upper bound. Note this can be computed in  $O(Nm^2)$  time.

As for NIP, we point out that  $\lambda y^\top (K + \sigma^2 I)^{-1} y$  is  $\min_{f \in \mathcal{H}} \sum_{i=1}^N (y_i - f(x_i))^2 + \lambda \|f\|_{\mathcal{H}}^2$ , the optimal value of the objective function in kernel ridge regression where  $\mathcal{H}$  is the Reproducing Kernel Hilbert Space associated with  $k$ . The dual problem, whose objective function has the same optimal value, is  $\max_{\alpha \in \mathbb{R}^N} -\lambda[\alpha^\top (K + \sigma^2 I)\alpha - 2\alpha^\top y]$ . So we have the upper bound:

$$-\frac{1}{2} y^\top (K + \sigma^2 I)^{-1} y \leq \frac{1}{2} \alpha^\top (K + \sigma^2 I)\alpha - \alpha^\top y \quad \forall \alpha \in \mathbb{R}^N \quad (4)$$

Note that this is also in the form of an objective for conjugate gradients(CG) [31], hence equality is obtained at the optimal value  $\hat{\alpha} = (K + \sigma^2 I)^{-1} y$ . We can approach the optimum for a tighter bound by using CG or preconditioned CG (PCG) for a fixed number of iterations to get a reasonable approximation to  $\hat{\alpha}$ . Each iteration of CG and the computation of the upper bound takes  $O(N^2)$  time, but PCG is very fast even for large data sets and FIC/PIC give fastest convergence in general [7]. Also recall that although the lower bound take  $O(Nm^2)$  to compute, we need  $m = O(N^\alpha)$  for accurate approximations, where  $\alpha$  depends on the data distribution and kernel [26].  $\alpha$  is usually close to 0.5, hence the lower bound is also effectively  $O(N^2)$ . Furthermore we only need to compute the upper bound once, whereas we must evaluate the lower bound and its gradients multiple times for the hyperparameter optimisation. We later confirm in Section 4.1 that the upper bound is fast to compute relative to the lower bound optimisation. We also show empirically that the upper bound is tighter than the lower bound in Section 4.1, and give the following sufficient condition for this to be true:

**Proposition 1.** *Suppose  $(\hat{\lambda}_i)_{i=1}^N$  are the eigenvalues of  $\hat{K} + \sigma^2 I$  in descending order. Then if (P)CG for the NIP term converges and  $\hat{\lambda}_N \geq 2\sigma^2$ , then the upper bound is tighter than the lower bound.*

Notice that  $\hat{\lambda}_N \geq \sigma^2 \quad \forall \hat{K}$ , so the assumption is feasible. The proof is in Appendix E.

We later show that the upper bound is not only tighter than the lower bound, but also much less sensitive to the choice of inducing points. Hence we use the upper bound to choose between kernels whose BIC intervals overlap.

### 3.3 SKC: Scalable Kernel Composition using the Lower and Upper Bound

Given a kernel and a value of  $m$ , we can compute the lower and upper bounds as above to obtain an interval for the exact GP marginal likelihood and hence the BIC of the kernel with its hyperparameters optimised by VAR. These hyperparameters may not be the global maximisers of the exact GP marginal likelihood, but as in ABCD we can optimise the marginal likelihood with multiple sets of random starting values to find the local optimum closest to the global optimum. One may still question whether the hyperparameter values found by VAR agree with the structure in the data, such as period values and slopes of linear trends. We show in Sections 4.2 and 4.3 that a small number of inducing points suffices for this to be the case.

---

**Algorithm 1:** Scalable Kernel Composition (SKC)

---

**Input:** data  $x_1, \dots, x_n \in \mathbb{R}^D, y_1, \dots, y_n \in \mathbb{R}$ , base kernel set  $\mathcal{B}$ , depth  $d$ , number of inducing points  $m$ , kernel buffer size  $S$   
**Output:**  $k$ , the resulting kernel

For each base kernel on each dimension, obtain lower and upper bounds to BIC (BIC interval), set  $k$  to be the kernel with highest upper bound, and add  $k$  to kernel buffer  $\mathcal{K}$ .  
 $\mathcal{C} \leftarrow \emptyset$   
**for**  $depth=1:d$  **do**  
    From  $\mathcal{C}$ , add to  $\mathcal{K}$  all kernels whose intervals overlap with  $k$  if there are fewer than  $S$  of them, else add the kernels with top  $S$  upper bounds.  
    **for**  $k' \in \mathcal{K}$  **do**  
        Add following kernels to  $\mathcal{C}$  and obtain their BIC intervals:  
        (1) All kernels of form  $k' + B$  where  $B$  is any base kernel on any dimension  
        (2) All kernels of form  $k' \times B$  where  $B$  is any base kernel on any dimension  
    **if exists kernel**  $k^* \in \mathcal{C}$  **with higher upper bound than**  $k$  **then**  
         $k \leftarrow k^*$

---

Note that we can guarantee that the lower bound increases with larger  $m$ , but cannot guarantee that the upper bound decreases. In fact, the upper bound is likely to increase as well, since with larger  $m$  it is likely that one finds hyperparameters that give a higher exact marginal likelihood from the lower bound optimisation, hence a higher upper bound. We verify this in Section 4.1. Hence for kernel evaluation, it would be sensible to use the largest possible value of  $m$  that one can afford, so that the exact marginal likelihood with hyperparameters optimised by VAR is as close as possible to the exact marginal likelihood with optimal hyperparameters.

With these intervals for each kernel, we can perform a semi-greedy kernel search whereby we expand the search tree on all (or some, controlled by buffer size  $S$ ) kernels whose intervals overlap with the top kernel at the current depth. See Figure 1 for a visualisation of the tree. Note that the algorithm is extremely parallelisable across different random initialisations and different kernels at each depth, hence very scalable not only in time complexity but also in practice (see Appendix F for further notes on parallelisation). Details on the optimisation and initialisation are given in Appendix G and H.

## 4 Experiments

### 4.1 Investigating the behaviour of the lower and upper bound

We present results for experiments showing the bounds we obtain for two small time series and a multidimensional regression data set, for which CKS is feasible. The first is the annual solar irradiance data from 1610 to 2011, with 402 observations [16]. The second is the time series Mauna Loa CO2 data<sup>3</sup> with 689 observations. See Appendix J for plots of the time series. The multidimensional data set is the concrete compressive strength data set with 1030 observations and 8 covariates<sup>4</sup>. The functional form of kernels used for each of these data sets have been found by CKS (see Figure 3). All observations and covariates have been normalised to have mean 0 and variance 1.

From the left of Figures 2a, 9a and 10a, (the latter two can be found in Appendix Q) we see that VAR gives a lower bound for the optimal log marginal likelihood that improves with increasing  $m$ . The best lower bound is tight relative to the exact log marginal likelihoods at the hyperparameters optimised by VAR, supporting the claim that VAR produces a strong lower bound. We also see that the upper bound is even tighter than the lower bound, and increases with  $m$  as hypothesised. In Appendix K we show further experimental evidence for a wider range of kernels reinforcing the claim that the upper bound is tighter than the lower bound, as well as being much less sensitive to the choice of inducing points. This is why the upper bound is a much more reliable metric for the model selection than the lower bound. From the middle plots, we observe that the Nyström approximation

---

<sup>3</sup>Data can be found at [ftp://ftp.cmdl.noaa.gov/ccg/co2/trends/co2\\_mm\\_mlo.txt](ftp://ftp.cmdl.noaa.gov/ccg/co2/trends/co2_mm_mlo.txt)

<sup>4</sup>Data can be found at <https://archive.ics.uci.edu/ml/datasets/Concrete+Compressive+Strength>

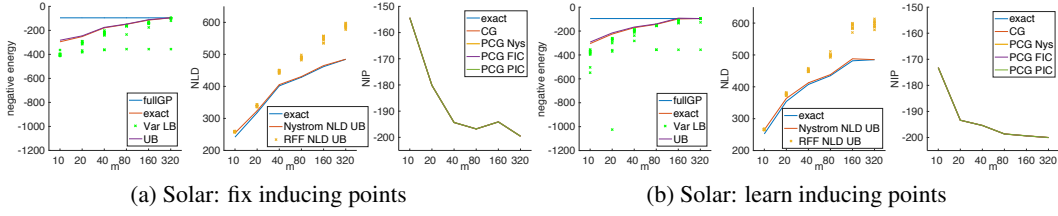


Figure 2: (a) Left: negative energy (log marginal likelihood + log prior) for fullGP with optimised hyperparameters, optimised VAR lower bound for each of 10 random initialisations per  $m$ , exact negative energy for best hyperparameters out of 10, and corresponding upper bound. Middle: exact NLD and upper bounds. Right: exact NIP and upper bounds after  $m$  iterations of CG/PCG. (b) Same as Figure 2a, except learning inducing points for the VAR lower bound optimisation and using them for subsequent computations.

gives a very tight upper bound on the NLD term. We also tried using RFF to get stochastic upper bounds (see Appendix P), but these are not as tight, especially for larger values of  $m$ . From the right plots, we can see that PCG with any of the three preconditioners (Nyström, FIC, PIC) give very tight upper bounds to the NIP term, whereas CG may require more iterations to get tight, for example in Figures 9a, 9b in Appendix Q.

Comparing Figures 2a, 9a, 10a against 2b, 9b, 10b, learning inducing points does not lead to a vast improvement in the VAR lower bound. In fact the differences are not very significant, and sometimes learning inducing points can get the lower bound stuck in a bad local minimum, as indicated by the high variance of lower bounds in the latter three figures. Moreover the differences in computational time is significant as we can see in Table 3 of Appendix I. Hence the computation-accuracy trade-off is best when fixing the inducing points to a random subset of training data.

Table 3 also compares times for the different computations after fixing the inducing points. The gains from using the variational lower bound instead of the full GP is clear, especially for the larger data sets, and we also confirm that it is indeed the optimisation of the LB that is the bottleneck in terms of computational cost. We also see that the NIP upper bound computation times are similarly fast for all  $m$ , thus convergence of PCG with the PIC preconditioner is happening in only a few iterations.

## 4.2 SKC on small data sets

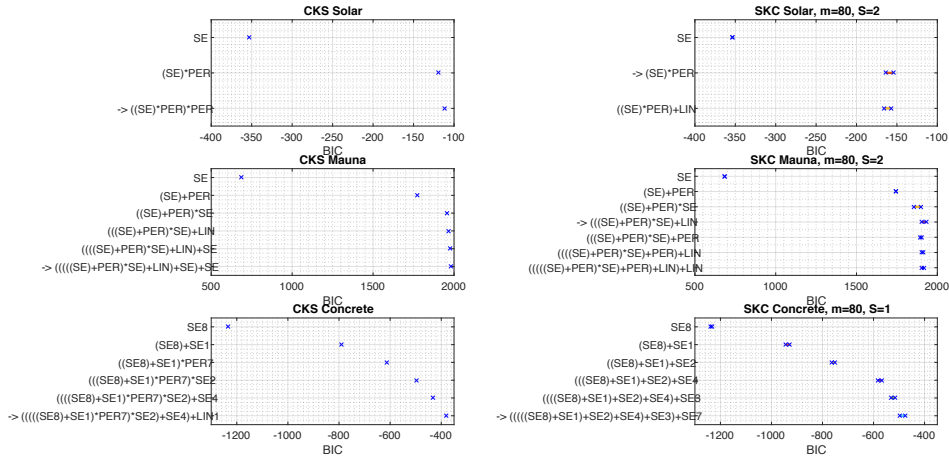


Figure 3: CKS & SKC results for up to depth 6. Left: BIC of kernels chosen at each depth by CKS. Right: BIC intervals of kernels that have been added to the buffer by SKC with  $m = 80$ . The arrow indicates the kernel chosen at the end.

We compare the kernels chosen by CKS and by SKC for the three data sets. The results are summarised in Figure 3. For solar, we see that the SKC successfully finds  $SE \times PER$ , which is the

second highest kernel for CKS, with BIC very close to the top kernel. For mauna, SKC selects  $(SE + PER) \times SE + LIN$ , which is third highest for CKS and a BIC very close to the top kernel. Looking at the values of hyperparameters in kernels PER and LIN found by SKC, 40 inducing points are sufficient for it to successfully find the correct periods and slopes in the data (see Appendix J for details). For concrete, a more challenging eight dimensional data set, we see that the kernels selected by SKC do not match those selected by CKS, but it still manages to find similar additive structure such as  $SE_1 + SE_8$  and  $SE_4$ . Also PER7 found by CKS is dubious, since it is unlikely that concrete compressive strength is a periodic function of fine aggregate density, the seventh covariate. Of course, the BIC intervals for kernels found by SKC are for hyperparameters found by VAR with  $m = 80$ , hence do not necessarily contain the optimal BIC of kernels in CKS. However the above results show that our method is still capable of selecting appropriate kernels even for low values of  $m$ , without having to home in to the optimal BIC using high values of  $m$ .

### 4.3 SKC on large data sets

We implement SKC on large time series data to explore whether it can successfully find known structure at different scales. Such large data sets occur frequently for hourly time series over several years, or daily time series over centuries.

**GEFCOM** First we use the energy load data set from the 2012 Global Energy Forecasting Competition [14], and hourly time series of energy load from 2004/01/01 to 2008/06/30, with 8 weeks of missing data, giving  $N = 38,070$ . Notice this data size is far beyond the scope of full GP optimisation in CKS.

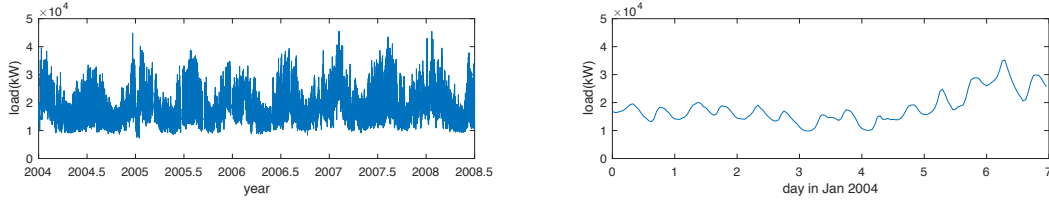


Figure 4: Left: Plot of full GEFCom data. Right: Zoom in for the first 7 days.

From the plots, we can see that there is a noisy 6-month periodicity in the time series, as well as a clear daily periodicity with peaks in the morning and evening. Despite the periodicity, there are some noticeable irregularities in the daily pattern.

Table 1: Kernel  $SE_1 \times PER_1 + SE_2 \times (PER_2 + LIN)$  found by SKC for  $m = 160$ , depth 6, after normalising  $y$ . Length scales, periods, and location converted to original scale,  $\sigma^2$  has been left as was found with normalised  $y$ .

	$SE_1$	$PER_1$	$SE_2$	$PER_2$	LIN
<b>Hyperparameters</b>	$\sigma^2 = 0.44$ $l = 60.5$ days	$\sigma^2 = 1.10$ $l = 1089$ days $p = 1.003$ days	$\sigma^2 = 0.18$ $l = 331$ days	$\sigma^2 = 0.06$ $l = 170$ days $p = 174$ days	$\sigma^2 = 0.17$ $loc = \text{year } 2006.1$

The kernel found by SKC with  $m = 160$  and its hyperparameters are summarised in Table 1. Note that just with 160 inducing points, SKC has successfully found the daily periodicity in  $PER_1$  and the 6-month periodicity in  $PER_2$ . The SE kernel in the first additive term suggests a local periodicity, exhibiting the irregular observation pattern that is repeated daily. Also note that the hyperparameter corresponding to the longer periodicity is close but not exactly half a year, owing to the noisiness of the periodicity that is apparent in the data. Moreover the magnitude of the second additive term  $SE_2 \times PER_2$  that contains the longer periodicity is  $0.18 \times 0.06$ , which is much smaller than the magnitude  $0.44 \times 1.10$  of the first additive term  $SE_1 \times PER_1$ . This explicitly shows that the second term has less effect than the first term on the behaviour of the time series, hence the weaker long-term periodicity.

**Tidal** We also run SKC on tidal data, namely the sea level measurements in Dover from 2013/01/03 to 2016/08/31<sup>5</sup>. This is an hourly time series, with each observation taken to be the mean of four readings taken every 15 minutes, giving  $N = 31,957$ .

<sup>5</sup>Data can be found at [https://www.bodc.ac.uk/data/hosted\\_data\\_systems/sea\\_level/uk\\_tide\\_gauge\\_network/processed/](https://www.bodc.ac.uk/data/hosted_data_systems/sea_level/uk_tide_gauge_network/processed/)

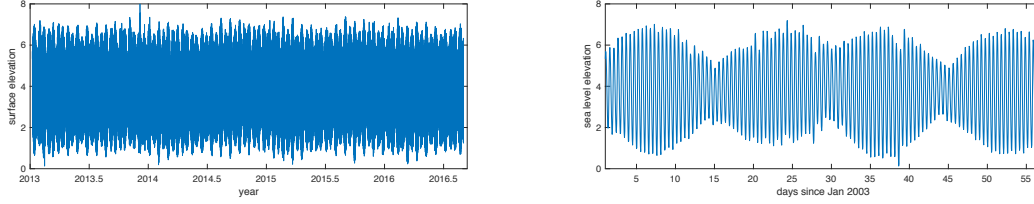


Figure 5: Left: Plot of full tidal data. Right: Zoom in for the first 4 weeks.

Looking at the right, we can find clear 12-hour periodicities along with amplitudes that follow slightly noisy bi-weekly periodicities. The shorter periods, called semi-diurnal tides, are in fact on average 12 hours 25 minutes  $\approx 0.518$  days long, and the bi-weekly periods arise due to gravitational effects of the moon [20].

Table 2: Kernel  $\text{SE} \times \text{PER}_1 \times \text{LIN} \times \text{SE}_2 \times \text{PER}_3$  found by SKC for  $m = 640$ , depth 5, after normalising  $y$ . Length scales, periods, and location converted to original scale,  $\sigma^2$  has been left as was found with normalised  $y$ .

	SE	$\text{PER}_1$	LIN	$\text{PER}_2$	$\text{PER}_3$
<b>Hyperparameters</b>	$\sigma^2 = 2.32$ $l = 82.5$ days	$\sigma^2 = 5.17$ $l = 1026$ days $p = 0.538$ days	$\sigma^2 = 0.18$ $loc = \text{year } 2015.0$	$\sigma^2 = 0.08$ $l = 5974$ days $p = 0.500$ days	$\sigma^2 = 0.21$ $l = 338$ days $p = 14.6$ days

The kernel found by SKC with  $m = 640$  and its hyperparameters are summarised in Table 2. The  $\text{PER}_1 \times \text{PER}_3$  kernel precisely corresponds to the doubly periodic structure in the data, whereby we have semi-daily periodicities with bi-weekly periodic amplitudes. The SE kernel has a length scale of 82.5 days, giving a local periodicity. This represents the irregularity of the amplitudes as can be observed on the right plot of Figure 5 between days 20 and 40. The LIN kernel has a large magnitude, but its effect is negligible when multiplied since the slope is calculated to be  $-5 \times 10^{-6}$  (see Appendix J for the slope calculation formula). It essentially has the role of boosting up the magnitude of the resulting kernel and hence representing noise in the data. The  $\text{PER}_2$  kernel is also negligible due to its high length scale, indicating that the amplitude of the periodicity due to this term is very small. Its magnitude is also small, hence the term has minimal effect on the kernel.

In both cases, SKC is able to detect the structure of data and provide accurate numerical estimates of its features, all with much fewer inducing points than  $N$ .

## 5 Conclusion and Discussion

We have introduced SKC, a scalable kernel discovery algorithm that extends CKS and hence ABCD to bigger data sets. We use a novel cheap upper bound to the GP marginal likelihood along with the variational lower bound in [34] to sandwich the marginal likelihood, using the interval for selecting between different kernels. The reasons for using an upper bound instead of just the lower bound for model selection are as follows: the upper bound allows for a semi-greedy approach, allowing us to explore a wider range of kernels and compensates for the suboptimality coming from local optima in the hyperparameter optimisation. Should we wish to restrict the range of kernels explored for computational efficiency, the upper bound turns out to be tighter and more stable than the lower bound, hence we may use the upper bound as a reliable tie-breaker for kernels with overlapping intervals. Equipped with this upper bound, our method is able to pinpoint global/local periodicities and linear trends in time series with tens of thousands of data points, which are well beyond the reach of its predecessor CKS in ABCD.

For future work we should look into making the algorithm even more scalable: for truly big data sets where even quadratic runtime is infeasible, we can apply stochastic variational inference for GPs [13] to optimise the lower bound, the bottleneck of SKC, using mini-batches of data. A corresponding upper bound that is tight enough for model selection would pose a challenging problem. Another minor scope for future work is using grid integration for evaluation of kernels, which would give a more accurate estimate of the model evidence than BIC. A related paper uses Laplace approximation instead of BIC for kernel evaluation in a similar kernel search context [18]. However Laplace approximation adds on an expensive Hessian term, for which it is unclear how one can obtain lower and upper bounds.



## Acknowledgments

HK and YWT’s research leading to these results has received funding from the European Research Council under the European Union’s Seventh Framework Programme (FP7/2007-2013) ERC grant agreement no. 617071.

## References

- [1] Francis R Bach, Gert RG Lanckriet, and Michael I Jordan. Multiple kernel learning, conic duality, and the smo algorithm. In *ICML*, 2004.
- [2] Rémy Bardenet and Michalis Titsias. Inference for determinantal point processes without spectral knowledge. *NIPS*, 2015.
- [3] Matthias Stephan Bauer, Mark van der Wilk, and Carl Edward Rasmussen. Understanding probabilistic sparse gaussian process approximations. *NIPS*, 2016.
- [4] Matthew James Beal. *Variational algorithms for approximate Bayesian inference*. PhD thesis, University College London, 2003.
- [5] Stephen Boyd and Lieven Vandenberghe. *Convex optimization*. Cambridge University Press, 2004.
- [6] Corinna Cortes, Mehryar Mohri, and Ameet Talwalkar. On the impact of kernel approximation on learning accuracy. In *AISTATS*, 2010.
- [7] Kurt Cutajar, Michael A. Osborne, John P. Cunningham, and Maurizio Filippone. Preconditioning kernel matrices. *ICML*, 2016.
- [8] Petros Drineas and Michael Mahoney. On the nyström method for approximating a gram matrix for improved kernel-based learning. *JMLR*, 6:2153–2175, 2005.
- [9] David Duvenaud, James Lloyd, Roger Grosse, Joshua Tenenbaum, and Ghahramani Zoubin. Structure discovery in nonparametric regression through compositional kernel search. In *ICML*, 2013.
- [10] Chris Fraley and Adrian E Raftery. Bayesian regularization for normal mixture estimation and model-based clustering. *Journal of classification*, 24(2):155–181, 2007.
- [11] Jacob Gardner, Chuan Guo, Kilian Weinberger, Roman Garnett, and Roger Grosse. Discovering and exploiting additive structure for bayesian optimization. In *AISTATS*, 2017.
- [12] Roger B. Grosse, Ruslan Salakhutdinov, William T. Freeman, and Joshua B. Tenenbaum. Exploiting compositionality to explore a large space of model structures. In *UAI*, 2012.
- [13] James Hensman, Nicolo Fusi, and Neil D Lawrence. Gaussian processes for big data. *arXiv preprint arXiv:1309.6835*, 2013.
- [14] Tao Hong, Pierre Pinson, and Shu Fan. Global energy forecasting competition 2012, 2014.
- [15] Chunlin Ji, Haige Shen, and Mike West. Bounded approximations for marginal likelihoods. 2010.
- [16] Judith Lean, Juerg Beer, and Raymond S Bradley. Reconstruction of solar irradiance since 1610: Implications for climate change. *Geophysical Research Letters*, 22(23), 1995.
- [17] James Robert Lloyd, David Duvenaud, Roger Grosse, Joshua Tenenbaum, and Zoubin Ghahramani. Automatic construction and natural-language description of nonparametric regression models. In *AAAI*, 2014.
- [18] Gustavo Malkomes, Charles Schaff, and Roman Garnett. Bayesian optimization for automated model selection. In *NIPS*, 2016.
- [19] Alexander G de G Matthews, James Hensman, Richard E Turner, and Zoubin Ghahramani. On sparse variational methods and the kullback-leibler divergence between stochastic processes. *AISTATS*, 2016.
- [20] John Morrissey, James L Sumich, and Deanna R. Pinkard-Meier. *Introduction To The Biology Of Marine Life*. Jones & Bartlett Learning, 1996.
- [21] Kevin P Murphy. *Machine learning: a probabilistic perspective*. MIT press, 2012.
- [22] Junier B Oliva, Avinava Dubey, Andrew G Wilson, Barnabás Póczos, Jeff Schneider, and Eric P Xing. Bayesian nonparametric kernel-learning. In *AISTATS*, 2016.
- [23] Joaquin Quinonero-Candela and Carl Edward Rasmussen. A unifying view of sparse approximate gaussian process regression. *JMLR*, 6:1939–1959, 2005.
- [24] Ali Rahimi and Benjamin Recht. Random features for large-scale kernel machines. In *NIPS*, 2007.
- [25] Carl Edward Rasmussen. *Gaussian processes for machine learning*. MIT Press, 2006.
- [26] Alessandro Rudi, Raffaello Camoriano, and Lorenzo Rosasco. Less is more: Nyström computational regularization. In *NIPS*, 2015.
- [27] Walter Rudin. Fourier analysis on groups. *AMS*, 1964.

- [28] Yves-Laurent Kom Samo and Stephen Roberts. Generalized spectral kernels. *arXiv preprint arXiv:1506.02236*, 2015.
- [29] Gideon Schwarz et al. Estimating the dimension of a model. *The Annals of Statistics*, 6(2):461–464, 1978.
- [30] Matthias Seeger, Christopher Williams, and Neil Lawrence. Fast forward selection to speed up sparse gaussian process regression. In *AISTATS*, 2003.
- [31] Jonathan Richard Shewchuk. An introduction to the conjugate gradient method without the agonizing pain, 1994.
- [32] Edward Snelson and Zoubin Ghahramani. Sparse gaussian processes using pseudo-inputs. In *NIPS*, 2005.
- [33] Arno Solin and Simo Särkkä. Explicit link between periodic covariance functions and state space models. *JMLR*, 2014.
- [34] Michalis K Titsias. Variational learning of inducing variables in sparse gaussian processes. In *AISTATS*, 2009.
- [35] Jarno Vanhatalo, Jaakko Riihimäki, Jouni Hartikainen, Pasi Jylänki, Ville Tolvanen, and Aki Vehtari. Gpstuff: Bayesian modeling with gaussian processes. *JMLR*, 14(Apr):1175–1179, 2013.
- [36] Christopher Williams and Matthias Seeger. Using the nyström method to speed up kernel machines. In *NIPS*, 2001.
- [37] Andrew Gordon Wilson and Ryan Prescott Adams. Gaussian process kernels for pattern discovery and extrapolation. *arXiv preprint arXiv:1302.4245*, 2013.
- [38] Andrew Gordon Wilson, Zhiting Hu, Ruslan Salakhutdinov, and Eric P Xing. Deep kernel learning. In *AISTATS*, 2016.

## A Bayesian Information Criterion (BIC)

The BIC is a model selection criterion that is the marginal likelihood with a model complexity penalty:

$$BIC = \log p(y|\hat{\theta}) - \frac{1}{2}p \log(N)$$

for observations  $y$ , number of observations  $N$ , maximum likelihood estimate (MLE) of model hyperparameters  $\hat{\theta}$ , number of hyperparameters  $p$ . It is derived as an approximation to the log model evidence  $\log p(y)$ .

## B Compositional Kernel Search Algorithm

---

### Algorithm 2: Compositional Kernel Search Algorithm

---

**Input:** data  $x_1, \dots, x_n \in \mathbb{R}^D, y_1, \dots, y_n \in \mathbb{R}$ , base kernel set  $\mathcal{B}$

**Output:**  $k$ , the resulting kernel

For each base kernel on each dimension, fit GP to data (i.e. optimise hyperparams by ML-II) and set  $k$  to be kernel with highest BIC.

**for**  $depth=1:T$  (either fix  $T$  or repeat until BIC no longer increases) **do**

    Fit GP to following kernels and set  $k$  to be the one with highest BIC:

- (1) All kernels of form  $k + B$  where  $B$  is any base kernel on any dimension
  - (2) All kernels of form  $k \times B$  where  $B$  is any base kernel on any dimension
  - (3) All kernels where a base kernel in  $k$  is replaced by another base kernel
- 

## C Base Kernels

$$\text{LIN}(x, x') = \sigma^2(x - l)(x' - l)$$

$$\text{SE}(x, x') = \sigma^2 \exp\left(-\frac{(x - x')^2}{2l^2}\right)$$

$$\text{PER}(x, x') = \sigma^2 \exp\left(-\frac{2 \sin^2(\pi(x - x')/p)}{l^2}\right)$$

## D Matrix Identities

**Lemma 1** (Woodbury's Matrix Inversion Lemma).  $(A + UBV)^{-1} = A^{-1} - A^{-1}U(B^{-1} + VA^{-1}U)^{-1}VA^{-1}$

**Lemma 2** (Sylvester's Determinant Theorem).  $\det(I + AB) = \det(I + BA) \quad \forall A \in \mathbb{R}^{m \times n} \quad \forall B \in \mathbb{R}^{n \times m}$

## E Proof of Proposition 1

*Proof.* If PCG converges, the upper bound for NIP is exact. We showed in Section 4.1 that the convergence happened in only a few iterations. Moreover [6] shows that the lower bound for NIP can be rather loose in general.

So it suffices to prove that the upper bound for NLD is tighter than the lower bound for NLD. Let  $(\lambda_i)_{i=1}^N, (\hat{\lambda}_i)_{i=1}^N$  be the ordered eigenvalues of  $K + \sigma^2 I, \hat{K} + \sigma^2 I$  respectively. Since  $K - \hat{K}$  is positive semi-definite (e.g. [2]), we have  $\lambda_i \geq \hat{\lambda}_i \geq 2\sigma^2 \forall i$  (using the assumption in the proposition). Now the slack in the upper bound is:

$$-\frac{1}{2} \log \det(\hat{K} + \sigma^2 I) - \left(-\frac{1}{2} \log \det(K + \sigma^2 I)\right) = \frac{1}{2} \sum_{i=1}^N (\log \lambda_i - \log \hat{\lambda}_i)$$

Hence the slack in the lower bound is:

$$-\frac{1}{2} \log \det(K + \sigma^2 I) - \left[ -\frac{1}{2} \log \det(\hat{K} + \sigma^2 I) - \frac{1}{2\sigma^2} \text{Tr}(K - \hat{K}) \right] = -\frac{1}{2} \sum_{i=1}^N (\log \lambda_i - \log \hat{\lambda}_i) + \frac{1}{2\sigma^2} \sum_{i=1}^N (\lambda_i - \hat{\lambda}_i)$$

Now by concavity and monotonicity of  $\log$ , and since  $\hat{\lambda} \geq 2\sigma^2$ , we have:

$$\begin{aligned} \frac{\log \lambda_i - \log \hat{\lambda}_i}{\lambda_i - \hat{\lambda}_i} &\leq \frac{1}{2\sigma^2} \\ \Rightarrow \sum_{i=1}^N (\log \lambda_i - \log \hat{\lambda}_i) &\leq \frac{1}{2\sigma^2} \sum_{i=1}^N (\lambda_i - \hat{\lambda}_i) \\ \Rightarrow \frac{1}{2} \sum_{i=1}^N (\log \lambda_i - \log \hat{\lambda}_i) &\leq \frac{1}{2\sigma^2} \sum_{i=1}^N (\lambda_i - \hat{\lambda}_i) - \frac{1}{2} \sum_{i=1}^N (\log \lambda_i - \log \hat{\lambda}_i) \end{aligned}$$

□

## F Parallelising SKC

Note that SKC can be parallelised across the random hyperparameter initialisations, and also across the kernels at each depth for computing the BIC intervals. In fact, SKC is even more parallelisable with the kernel buffer: say at a certain depth, we have two kernels that we are waiting to finish so that we can move onto the next depth. If the buffer size is 5, say, then we can in fact move on to the next depth and grow the kernel search tree on the top 3 kernels of the buffer, without having to wait for the 2 kernel evaluations to be complete. This saves a lot of computation time wasted by idle cores waiting for all kernel evaluations to finish before moving on to the next depth of the kernel search tree.

## G Optimisation

Since we wish to use the learned kernels for interpretation, it is important to have the hyperparameters lie in a sensible region after the optimisation. In other words, we wish to regularise the hyperparameters during optimisation. For example, we want the SE kernel to learn a globally smooth function with local variation. When naively optimising the lower bound, sometimes the length scale and the signal variance becomes very small, so the SE kernel explains all the variation in the signal and ends up connecting the dots. We wish to avoid this type of behaviour. This can be achieved by giving priors to hyperparameters and optimising the energy (log prior added to the log marginal likelihood) instead, as well as using sensible initialisations. Looking at Figure 6, we see that using a strong prior with a sensible random initialisation (see Appendix H for details) gives a sensible smoothly varying function, whereas for all the three other cases, we have the length scale and signal variance shrinking to small values, causing the GP to overfit to the data. Note that the weak prior is the default prior used in the GPstuff software [35].

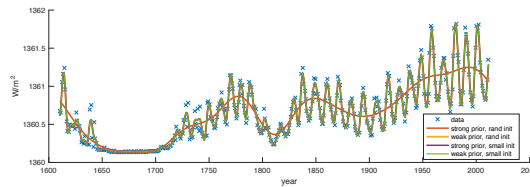


Figure 6: GP predictions on solar data set with SE kernel for different priors and initialisations.

Careful initialisation of hyperparameters and inducing points is also very important, and can have strong influence the resulting optima. It is sensible to have the optimised hyperparameters of the parent kernel in the search tree be inherited and used to initialise the hyperparameters of the child. The new hyperparameters of the child must be initialised with random restarts, where the variance is small enough to ensure that they lie in a sensible region, but large enough to explore a good portion of this region. As for the inducing points, we want to spread them out to capture both local and

global structure. Trying both K-means and a random subset of training data, we conclude that they give similar results and resort to a random subset. Moreover we also have the option of learning the inducing points. However, this will be considerably more costly and show little improvement over fixing them, as we show in Section 4. Hence we do not learn the inducing points, but fix them to a given randomly chosen set.

Hence for SKC, we use *maximum a posteriori* (MAP) estimates instead of MLE for the hyperparameters to calculate the BIC, since the priors have a noticeable effect on the optimisation. This is justified [21] and has been used for example in [10], where they argue that using the MLE to estimate the BIC for Gaussian mixture models can fail due to singularities and degeneracies.

## H Hyperparameter initialisation and priors

$Z \sim \mathcal{N}(0, 1)$ ,  $TN(\sigma^2, I)$  is a Gaussian with mean 0 and variance  $\sigma^2$  truncated at the interval  $I$  then renormalised.

### Signal noise

$$\sigma^2 = 0.1 \times \exp(Z/2)$$

$$p(\log \sigma^2) = \mathcal{N}(0, 0.2)$$

### LIN

$$\sigma^2 = \exp(V) \text{ where } V \sim TN(1, [-\infty, 0]), l = \exp(\frac{Z}{2})$$

$$p(\log \sigma^2) = \text{logunif}$$

$$p(\log l) = \text{logunif}$$

### SE

$$l = \exp(Z/2), \sigma^2 = 0.1 \times \exp(Z/2)$$

$$p(\log l) = \mathcal{N}(0, 0.01), p(\log \sigma^2) = \text{logunif}$$

### PER

$$p_{min} = \log(10 \times \frac{\max(x) - \min(x)}{N}) \text{ (shortest possible period is 10 time steps)}$$

$$p_{max} = \log(\frac{\max(x) - \min(x)}{5}) \text{ (longest possible period is a fifth of the range of data set)}$$

$$l = \exp(Z/2), p = \exp(p_{min} + W) \text{ or } \exp(p_{max} + U), \sigma^2 = 0.1 \times \exp(Z/2) \text{ w.p. } \frac{1}{2}$$

where  $W \sim \mathcal{TN}(-0.5, [0, \infty]), U \sim \mathcal{TN}(-0.5, [-\infty, 0])$

$$p(\log l) = t(\mu = 0, \sigma^2 = 1, \nu = 4), p(\log p) = \mathcal{LN}(p_{min} - 0.5, 0.25) \text{ or}$$

$$p(\log p) = \mathcal{LN}(p_{max} - 2, 0.5) \text{ w.p. } \frac{1}{2}$$

$$p(\log \sigma^2) = \text{logunif} \text{ where } \mathcal{LN}(\mu, \sigma^2) \text{ is log Gaussian, } t(\mu, \sigma^2, \nu) \text{ is the student's t-distribution.}$$

## I Computation Times for lower and upper bounds

Table 3: Mean and standard deviation of computation times (in seconds) for full GP optimisation, Var GP optimisation, NLD and NIP (PCG using PIC preconditioner) upper bounds over 10 random iterations.

	Solar	Mauna	Concrete
<b>GP</b>	29.1950 $\pm$ 5.1430	164.8828 $\pm$ 58.7865	403.8233 $\pm$ 127.0364
<b>Var GP</b>			
m=10	7.0259 $\pm$ 4.3928	6.0117 $\pm$ 3.8267	5.4358 $\pm$ 0.7298
m=20	8.3121 $\pm$ 5.4763	11.9245 $\pm$ 6.8790	10.2410 $\pm$ 2.5109
m=40	10.2263 $\pm$ 4.1025	17.1479 $\pm$ 10.7898	19.6678 $\pm$ 4.3924
m=80	9.6752 $\pm$ 6.5343	28.9876 $\pm$ 13.0031	47.2225 $\pm$ 13.1955
m=160	25.6330 $\pm$ 8.7934	91.0406 $\pm$ 39.8409	158.9199 $\pm$ 18.1276
m=320	76.3447 $\pm$ 20.3337	202.2369 $\pm$ 96.0749	541.4835 $\pm$ 99.6145
<b>NLD</b>			
m=10	0.0019 $\pm$ 0.0001	0.0033 $\pm$ 0.0002	0.0113 $\pm$ 0.0004
m=20	0.0026 $\pm$ 0.0001	0.0046 $\pm$ 0.0002	0.0166 $\pm$ 0.0007
m=40	0.0043 $\pm$ 0.0001	0.0079 $\pm$ 0.0003	0.0286 $\pm$ 0.0005
m=80	0.0084 $\pm$ 0.0002	0.0154 $\pm$ 0.0004	0.0554 $\pm$ 0.0012
m=160	0.0188 $\pm$ 0.0006	0.0338 $\pm$ 0.0007	0.1188 $\pm$ 0.0030
m=320	0.0464 $\pm$ 0.0032	0.0789 $\pm$ 0.0036	0.2550 $\pm$ 0.0074
<b>NIP</b>			
m=10	0.0474 $\pm$ 0.0092	0.1020 $\pm$ 0.0296	0.2342 $\pm$ 0.0206
m=20	0.0422 $\pm$ 0.0130	0.1274 $\pm$ 0.0674	0.1746 $\pm$ 0.0450
m=40	0.0284 $\pm$ 0.0075	0.0846 $\pm$ 0.0430	0.2345 $\pm$ 0.0483
m=80	0.0199 $\pm$ 0.0081	0.0553 $\pm$ 0.0250	0.2176 $\pm$ 0.0376
m=160	0.0206 $\pm$ 0.0053	0.0432 $\pm$ 0.0109	0.2136 $\pm$ 0.0422
m=320	0.0250 $\pm$ 0.0019	0.0676 $\pm$ 0.0668	0.2295 $\pm$ 0.0433
<b>Var GP, learn IP</b>			
m=10	23.4 $\pm$ 14.6	42.0 $\pm$ 33.0	110.0 $\pm$ 302.5
m=20	38.5 $\pm$ 17.5	62.0 $\pm$ 66.0	70.0 $\pm$ 97.0
m=40	124.7 $\pm$ 99.0	320.0 $\pm$ 236.0	307.0 $\pm$ 341.4
m=80	268.6 $\pm$ 196.6	1935.0 $\pm$ 1103.0	666.0 $\pm$ 41.0
m=160	1483.6 $\pm$ 773.8	10480.0 $\pm$ 5991.0	4786.0 $\pm$ 406.9
m=320	2923.8 $\pm$ 1573.5	39789.0 $\pm$ 23870.0	25906.0 $\pm$ 820.9

## J Mauna and Solar plots and hyperparameter values found by SKC

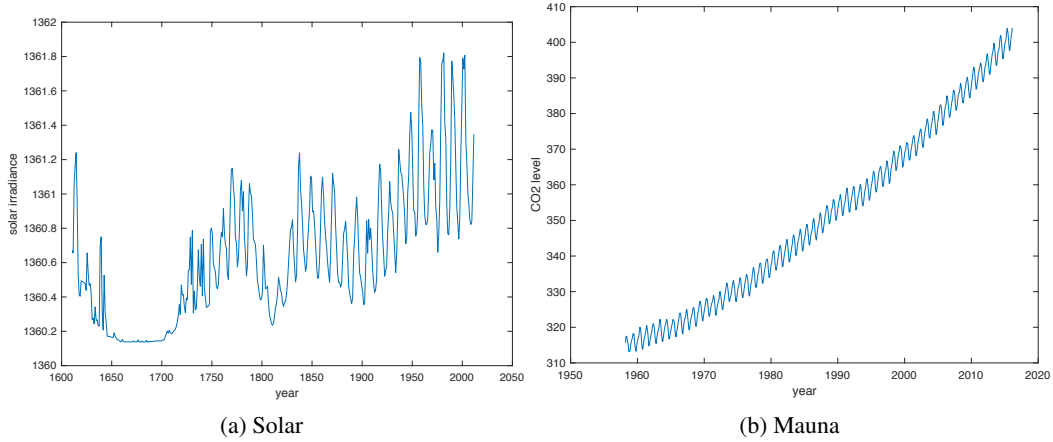


Figure 7: Plots of small time series data: Solar and Mauna

**Solar** The solar data has 26 cycles over 285 years, which gives a periodicity of around 10.9615 years. Using SKC with  $m = 40$ , we find the kernel:  $SE \times PER \times SE \equiv SE \times PER$ . The value of the period hyperparameter in PER is 10.9569 years, hence SKC finds the periodicity to 3 s.f. with only 40 inducing points. The SE term converts the global periodicity to local periodicity, with the extent of the locality governed by the length scale parameter in SE, equal to 45. This is fairly large, but smaller than the range of the domain (1610-2011), indicating that the periodicity spans over a long time but isn't quite global. This is most likely due to the static solar irradiance between the years 1650-1700, adding a bit of noise to the periodicities.

**Mauna** The annual periodicity in the data and the linear trend with positive slope is clear. Linear regression gives us a slope of 1.5149. SKC with  $m = 40$  gives the kernel: SE + PER + LIN. The period hyperparameter in PER takes value 1, hence SKC successfully finds the right periodicity. The offset  $l$  and magnitude  $\sigma^2$  parameters of LIN allow us to calculate the slope by the formula  $\sigma^2(x-l)^\top [\sigma^2(x-l)(x-l)^\top + \sigma_n^2 I]^{-1} y$  where  $\sigma_n^2$  is the noise variance in the learned likelihood. This formula is obtained from the posterior mean of the GP, which is linear in the inputs for the linear kernel. This value amounts to 1.5150, hence the slope found by SKC is accurate to 3 s.f.

## K Behaviour of the lower and upper bound when varying inducing points for fixed hyperparameters

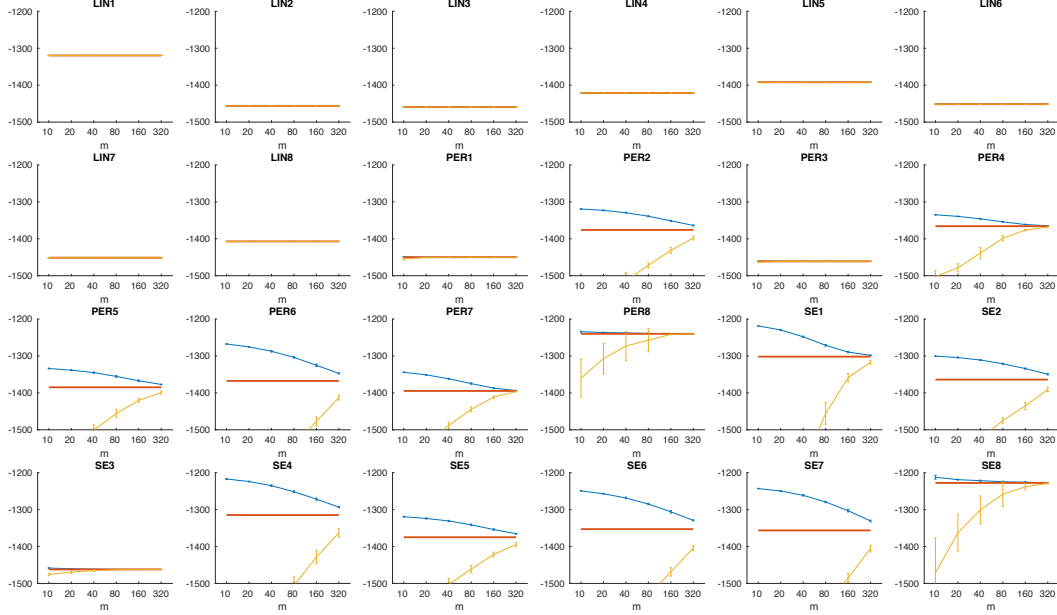


Figure 8: Upper and lower bounds for kernels at depth 1 on concrete data, with hyperparameters fixed to the optimal ones for the full GP and varying the inducing points. The error bars show mean  $\pm 1$  standard deviation over 10 random sets of inducing points.

From the plots, we observe that given hyperparameters, the upper bound is tighter, more stable and much less sensitive to the choice of inducing points compared to the lower bound. Hence for a one off comparison of kernels when their BIC intervals overlap, it is much more sensible to use the upper bound rather than the lower bound. However comparing with Figure 12 in Appendix Q that visualises the lower and upper bounds in the kernel search tree, we see that when we optimise the lower bound it becomes fairly tight. So it is also the case that given inducing points, the lower bound is sensitive to the choice of hyperparameters. In other words, the choice of hyperparameters and inducing points is important, but choosing inducing points randomly and optimising the hyperparameters gives a lower bound tight enough to the exact marginal likelihood with optimal hyperparameters.

## L Optimising the upper bound

If the upper bound is tighter and more robust with respect to choice of inducing points, why don't we optimise the upper bound to find hyperparameters? If this were to be possible then we can maximise this to get an upper bound of the exact marginal likelihood with optimal hyperparameters. In fact this holds for any analytic upper bound whose value and gradients can be evaluated cheaply. Hence for any  $m$ , we can find an interval that contains the true optimised marginal likelihood. So if this interval is dominated by an interval of another kernel, we can discard the kernel and there is no need to evaluate the bounds for bigger values of  $m$ . Now we wish to use values of  $m$  such that we can

choose the right kernel (or kernels) at each depth of the search tree with minimal computation. This gives rise to an exploitation-exploration trade-off, whereby we want to balance between raising  $m$  for tight intervals that allow us to discard unsuitable kernels whose intervals fall strictly below that of other kernels, and quickly moving on to the next depth in the search tree to search for finer structure in the data. The search algorithm is highly parallelisable, and thus we may raise  $m$  simultaneously for all candidate kernels. At deeper levels of the search tree, there may be too many candidates for simultaneous computation, in which case we may select the ones with the highest upper bound to get tighter intervals. Such attempts are listed below.

Note the two inequalities for the NLD and NIP terms:

$$\begin{aligned} -\frac{1}{2} \log \det(\hat{K} + \sigma^2 I) - \frac{1}{2\sigma^2} \text{Tr}(K - \hat{K}) &\leq -\frac{1}{2} \log \det(K + \sigma^2 I) \leq -\frac{1}{2} \log \det(\hat{K} + \sigma^2 I) \\ -\frac{1}{2} y^\top (\hat{K} + \sigma^2 I)^{-1} y &\leq -\frac{1}{2} y^\top (K + \sigma^2 I)^{-1} y \leq -\frac{1}{2} y^\top (K + (\sigma^2 + \text{Tr}(K - \hat{K}))I)^{-1} y \end{aligned}$$

Where the first two inequalities come from [2], the third inequality is a direct consequence of  $K - \hat{K}$  being positive semi-definite, and the last inequality is from Michalis Titsias' lecture slides <sup>6</sup>.

Also from 4, we have that

$$-\frac{1}{2} \log \det(\hat{K} + \sigma^2 I) + \frac{1}{2} \alpha^\top (K + \sigma^2 I) \alpha - \alpha^\top y$$

is an upper bound  $\forall \alpha \in \mathbb{R}^N$ . Thus one idea of obtaining a cheap upper bound to the optimised marginal likelihood was to solve the following maximin optimisation problem:

$$\max_{\theta} \min_{\alpha \in \mathbb{R}^N} -\frac{1}{2} \log \det(\hat{K} + \sigma^2 I) + \frac{1}{2} \alpha^\top (K + \sigma^2 I) \alpha - \alpha^\top y$$

One way to solve this cheaply would be by coordinate descent, where one maximises with respect to  $\theta$  fixing  $\alpha$ , then minimises with respect to  $\alpha$  fixing  $\theta$ . However  $\sigma$  tends to blow up in practice. This is because the expression is  $O(-\log \sigma^2 + \sigma^2)$  for fixed  $\alpha$ , hence maximising with respect to  $\sigma$  pushes it towards infinity.

An alternative is to sum the two upper bounds above to get the upper bound

$$-\frac{1}{2} \log \det(\hat{K} + \sigma^2 I) - \frac{1}{2} y^\top (K + (\sigma^2 + \text{Tr}(K - \hat{K}))I)^{-1} y$$

However we found that maximising this bound gives quite a loose upper bound unless  $m = O(N)$ . Hence this upper bound is not very useful.

## M Random Fourier Features

Random Fourier Features (RFF) (a.k.a. Random Kitchen Sinks) was introduced by [24] as a low rank approximation to the kernel matrix. It uses the following theorem

**Theorem 3** (Bochner's Theorem [27]). *A stationary kernel  $k(d)$  is positive definite if and only if  $k(d)$  is the Fourier transform of a non-negative measure.*

to give an unbiased low-rank approximation to the Gram matrix  $K = \mathbb{E}[\Phi^\top \Phi]$  with  $\Phi \in \mathbb{R}^{m \times N}$ . A bigger  $m$  lowers the variance of the estimate. Using this approximation, one can compute determinants and inverses in  $O(Nm^2)$  time. In the context of kernel composition in 2, RFFs have the nice property that samples from the spectral density of the sum or product of kernels can easily be obtained as sums or mixtures of samples of the individual kernels (see Appendix N). We use this later to give a memory-efficient upper bound on the exact log marginal likelihood in Appendix P.

<sup>6</sup><http://www.aueb.gr/users/mtitsias/papers/titsiasNipsVar14.pdf>



## N Random Features for Sums and Products of Kernels

For RFF the kernel can be approximated by the inner product of random features given by samples from its spectral density, in a Monte Carlo approximation, as follows:

$$\begin{aligned}
 k(x - y) &= \int_{\mathbb{R}^D} e^{iv^\top(x-y)} d\mathbb{P}(v) \propto \int_{\mathbb{R}^D} p(v) e^{iv^\top(x-y)} dv = \mathbb{E}_{p(v)}[e^{iv^\top x} (e^{iv^\top y})^*] \\
 &= \mathbb{E}_{p(v)}[Re(e^{iv^\top x} (e^{iv^\top y})^*)] \\
 &\approx \frac{1}{m} \sum_{k=1}^m Re(e^{iv_k^\top x} (e^{iv_k^\top y})^*) \\
 &= \mathbb{E}_{b,v}[\phi(x)^\top \phi(y)]
 \end{aligned}$$

where  $\phi(x) = \sqrt{\frac{2}{m}}(\cos(v_1^\top x + b_1), \dots, \cos(v_m^\top x + b_m))$  with spectral frequencies  $v_k$  iid samples from  $p(v)$  and  $b_k$  iid samples from  $U[0, 2\pi]$ .

Let  $k_1, k_2$  be two stationary kernels, with respective spectral densities  $p_1, p_2$  so that

$k_1(d) = a_1 \hat{p}_1(d), k_2(d) = a_2 \hat{p}_2(d)$ , where  $\hat{p}(d) := \int_{\mathbb{R}^D} p(v) e^{iv^\top d} dv$ . We use this convention as the Fourier transform. Note  $a_i = k_i(0)$ .

$$(k_1 + k_2)(d) = a_1 \int p_1(v) e^{iv^\top d} dv + a_2 \int p_2(v) e^{iv^\top d} dv = (a_1 + a_2) \hat{p}_+(d)$$

where  $p_+(v) = \frac{a_1}{a_1+a_2} p_1(v) + \frac{a_2}{a_1+a_2} p_2(v)$ , a mixture of  $p_1$  and  $p_2$ . So to generate RFF for  $k_1 + k_2$ , generate  $v \sim p_+$  by generating  $v \sim p_1$  w.p.  $\frac{a_1}{a_1+a_2}$  and  $v \sim p_2$  w.p.  $\frac{a_2}{a_1+a_2}$

Now for the product, suppose

$$(k_1 \cdot k_2)(d) = a_1 a_2 \hat{p}_1(d) \hat{p}_2(d) = a_1 a_2 \hat{p}_*(d)$$

Then  $p_*(d)$  is the inverse fourier transform of  $\hat{p}_1 \hat{p}_2$ , which is the convolution  $p_1 * p_2(d) := \int_{\mathbb{R}^D} p_1(z) p_2(d-z) dz$ . So to generate RFF for  $k_1 \cdot k_2$ , generate  $v \sim p_*$  by generating  $v_1 \sim p_1, v_2 \sim p_2$  and setting  $v = v_1 + v_2$ .

This is not applicable for non-stationary kernels, such as the linear kernel. We deal with this problem as follows:

Suppose  $\phi_1, \phi_2$  are random features such that

$$k_1(x, x') = \phi_1(x)^\top \phi_1(x'), \phi_2(x)^\top \phi_2(x'), \phi_i : \mathbb{R}^D \rightarrow \mathbb{R}^m.$$

It is straightforward to verify that

$$\begin{aligned}
 (k_1 + k_2)(x, x') &= \phi_+(x)^\top \phi_+(x') \text{ where } \phi_+(\cdot) = (\phi_1(\cdot)^\top, \phi_2(\cdot)^\top)^\top \\
 (k_1 \cdot k_2)(x, x') &= \phi_*(x)^\top \phi_*(x') \text{ where } \phi_*(\cdot) = \phi_1(\cdot) \otimes \phi_2(\cdot)
 \end{aligned}$$

However we do not want the number of features to grow as we add or multiply kernels, since it will grow exponentially. We want to keep it to be  $m$  features. So we subsample  $m$  entries from  $\phi_+$  (or  $\phi_*$ ) and scale by factor  $\sqrt{2}$  ( $\sqrt{m}$  for  $\phi_*$ ), which will still give us unbiased estimates of the kernel provided that each term of the inner product  $\phi_+(x)^\top \phi_+(x')$  (or  $\phi_*(x)^\top \phi_*(x')$ ) is an unbiased estimate of  $(k_1 + k_2)(x, x')$  (or  $(k_1 \cdot k_2)(x, x')$ ).

This is how we generate random features for linear kernels combined with other stationary kernels, using the features  $\phi(x) = \frac{\sigma}{\sqrt{m}}(x, \dots, x)^\top$ .

## O Spectral Density for PER

From [33], we have that the spectral density of the PER kernel is:

$$\sum_{n=-\infty}^{\infty} \frac{I_n(l^{-2})}{\exp(l^{-2})} \delta\left(v - \frac{2\pi n}{p}\right)$$

where  $I$  is the modified Bessel function of the first kind.

## P An upper bound to NLD using Random Fourier Features

Note that the function  $f(X) = -\log \det(X)$  is convex on the set of positive definite matrices [5]. Hence by Jensen's inequality we have, for  $\Phi^\top \Phi$  an unbiased estimate of  $K$ :

$$-\frac{1}{2} \log \det(K + \sigma^2 I) = f(K + \sigma^2 I) = f(\mathbb{E}[\Phi^\top \Phi + \sigma^2 I]) \leq \mathbb{E}[f(\Phi^\top \Phi + \sigma^2 I)] \quad (5)$$

Hence  $-\frac{1}{2} \log \det(\Phi^\top \Phi + \sigma^2 I)$  is a stochastic upper bound to NLD that can be calculated in  $O(Nm^2)$ . An example of such an unbiased estimator  $\Phi$  is given by RFF.

## Q Further Plots

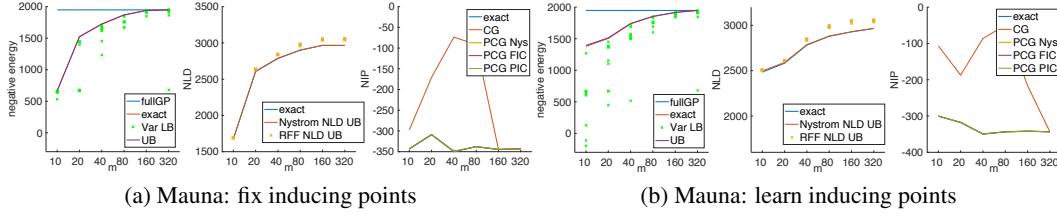


Figure 9: Same as 2a and 2b but for Mauna Loa data.

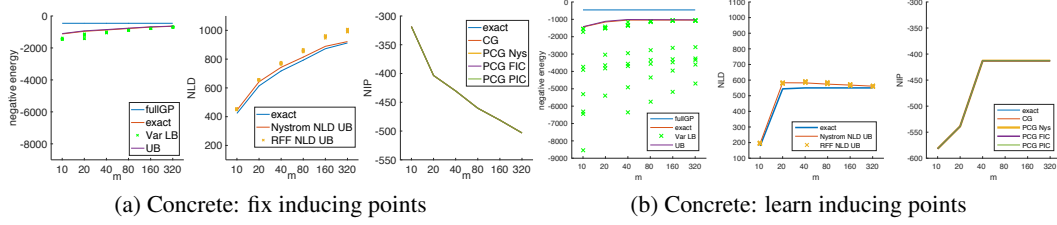


Figure 10: Same as 2a and 2b but for Concrete data.

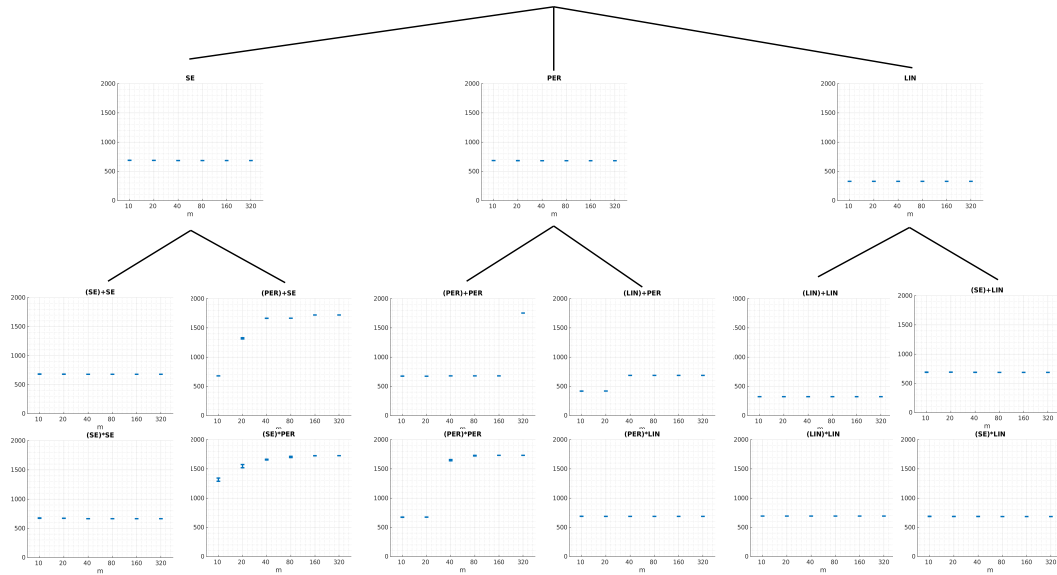


Figure 11: Same as Figure 1 but for Mauna data.

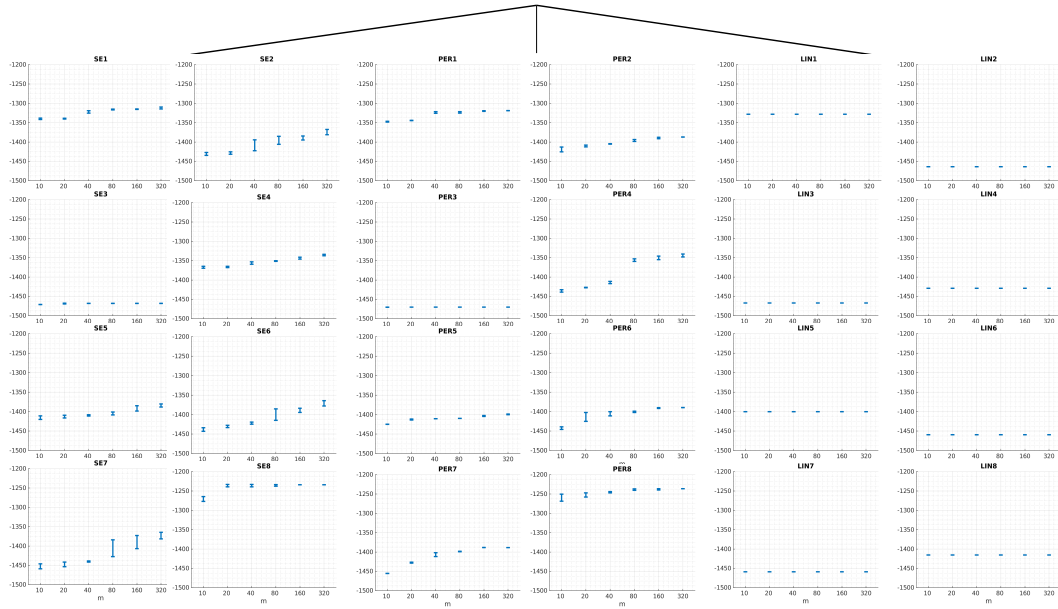


Figure 12: Same as Figure 1 but for concrete data and up to depth 1.